Estimation of Phytoplankton Chlorophyll-a Concentrations in the Western Basin of Lake Erie Using Sentinel-2 and Sentinel-3 Data

Saied Pirasteh , Somayeh Mollaee , Sarah Narges Fatholahi & Jonathan Li

Published online: 24 Sep 2020.

Submit your article to this journal

View related articles

View Crossmark data

Check for updates

Estimation of Phytoplankton Chlorophyll-a Concentrations in the Western Basin of Lake Erie Using Sentinel-2 and Sentinel-3 Data

Estimation des concentrations de chlorophylle-a du phytoplancton dans le bassin Ouest du Lac Érié à l'aide des données Sentinel-2 et Sentinel-3

Saied Pirasteh[a,b] (iD), Somayeh Mollaee[b], Sarah Narges Fatholahi[b] (iD), and Jonathan Li[b,c] (iD)

[a]Faculty of Geosciences and Environmental Engineering, Southwest Jiaotong University, Chengdu 611756, China; [b]Department of Geography and Environmental Management, University of Waterloo, Waterloo N2L 3G1, Canada; [c]Department of Systems Design Engineering, University of Waterloo, Waterloo N2L 3G1, Canada

ABSTRACT

Algae blooms have been a serious problem in coastal and inland water bodies across Canada. The temporal and spatial variability of algae blooms makes it difficult to use *in situ* monitoring of the lakes. This study aimed to evaluate the potential of Sentinel-3 Ocean and Land Color Instrument (OLCI) and Sentinel-2 Multispectral Instrument (MSI) data for monitoring algal blooms in Lake Erie. Chlorophyll-a (Chl-a)-related products of these sensors were tested by using the Great Lakes Chl-a NOAA's monitoring data over summer 2016 and 2017, respectively. Our results show that while fluorescent light height (FLH) algorithm and models are limited to lakes with Chl-a $< 8\,mg/m^3$, maximum chlorophyll index (MCI) has the potential to be used effectively to monitor Chl-a concentration over Eutrophic lakes. Sentinel-3's MCI is suggested for Chl-a $> 20\,mg/m^3$ and Sentinel-2 MCI for Chla $> 8\,mg/m^3$. Top of atmosphere (TOA) radiances showed a significantly better correlation with *in situ* data compared to TOA reflectance, which may be related to the poor pixel identification during the process of pixel flagging affected by the complexity of Case-2 water. Sentinel-2 MCI achieves better performance for Chl-a retrieval ($R^2 = 0.92$) than the existing methods. However, the FLH algorithms outperformed negative reflectance due to the shift of reflectance peak to longer wavelengths along with increasing Chl-a values.

RÉSUMÉ

La prolifération d'algues est un problème important dans les eaux côtières et intérieures du Canada. La variabilité temporelle et spatiale des floraisons d'algues rend difficile la surveillance *in situ* des lacs. Cette étude vise à évaluer le potentiel des données acquises par les capteurs 'Ocean and Land Color Instrument (OLCI)' de Sentinel-3 et 'Multispectral Instrument (MSI)' de Sentinel-2 pour la surveillance des efflorescences algales dans le lac Érié. Leurs produits liés à la chlorophylle-a (Chl-a) ont été testés à l'aide des données de surveillance du Chl-a de la NOAA dans les Grands Lacs au cours des étés 2016 et 2017, respectivement. Nos résultats montrent que les algorithmes de FLH sont limités aux lacs dont la concentration en Chl-a est inférieure à 8 mg/m3, l'indice MCI peut être utilisé efficacement pour surveiller la concentration en Chl-a dans les lacs eutrophiques. L'indice MCI de Sentinel-3 est suggéré pour Chl-a > 20 mg/m3 et celui de Sentinel-2 pour Chla > 8 mg/m3. Ces valeurs de concentration différentes pour les produits MCI peuvent être dues aux emplacements des réflectances maximums, c.-à-d., 705 nm et 709 nm, pour les capteurs MSI et OLCI, respectivement. Les radiances TOA ont montré une corrélation significativement meilleure avec les données *in situ* par rapport à la réflectance TOA, ce qui peut être lié à une mauvaise identification des pixels pendant le processus de marquage due à la complexité de l'eau dans le cas de l'étude 2. Des meilleures performances ont été atteintes par l'indice MCI de Sentinel-2 (R2 = 0.92) que par les méthodes existantes. Cependant, les algorithmes FLH ont surpassé la réflectance négative en raison du déplacement du maximum de la réflectance vers des longueurs d'onde plus longues avec des concentrations de Chl-a croissantes.

CONTACT Saied Pirasteh ✉ sapirasteh@swjtu.edu.cn; Jonathan Li ✉ junli@uwaterloo.ca

Introduction and background

Lakes offer essential ecological, environmental, hydrology, and socioeconomic services. These habitats provide food supply, water supply, and have enormous biodiversity in addition to carrying out climate, hydrological, and biogeochemical regulation and pollution control. Environmental changes such as climate, land cover, and development pressure, in particular deforestation, lost vegetation cover, increased nutrient runoff, urbanization, and watershed modification, have rapidly degraded water quality. These changes and pressures cause eutrophication,[1] increased turbidity, deterioration of water clarity, and loss of aquatic benthos (Binding et al. 2013; Olmanson et al. 2008; Palmer et al. 2015; Wang and Shi 2007; Witter et al. 2009).

Moreover, they make a risk for human and animal health. Therefore, the management and monitoring of lakes should be a priority of environmental resource management, which needs a low cost and effective program. To make this plan successful, in addition to regularly ground-based monitoring methods, a cost-efficient, high spatial and temporal coverage method is a demand and remotely sensed satellite images are a powerful tool for this (Amanollahi et al. 2012; Blondeau-Patissier et al. 2014; Devred et al. 2013; Hill et al. 2014; Kutser et al. 2005; Palmer et al. 2015).

The idea of using remote sensing for water monitoring emerged in the 1960s. The aim was to study ocean color with the assumption of the possibility to estimate chlorophyll-a (Chl-a) as a proxy of phytoplankton and sea surface temperature (SST) via a remote sensing technique (Gordon et al. 1975, 1988). On the basis of this perception, researchers started to estimate optically active constituents (OACs), such as colored dissolved matters (CDOMs), suspended particles, and phytoplankton remotely (Jerlov 1976). Subsequently, the concept of ocean optics and the theory of the radiative transfer equation (RTE) were developed and became the basis of bio-optical modeling. Nevertheless, the application of these theories and techniques has only been used less than 30 years for inland waters, which are different compared to oceans. Morel and Prieur (1977) suggested two different classes of water: Case I and Case II base on the ratios of 443 nm and 550 nm (higher than 1.0 assumed Case I and less than 1.0 Case II). A newer assumption by Gordon and Morel (2012) was that Case I water optical properties are mainly controlled by phytoplankton, where Case II water is dominated by other water constituents such as CDOM and Nan-Algae Particle (NAP). However, the main criticism of this assumption is that inland water can be dominated by phytoplankton that can be assumed Case I. Nevertheless, this classification is useful in having a view of two water types.

Absorption and scattering characteristics

The absorption and scattering properties of water are the foundation for the use of the optical remote sensing (ORS) system to measure water constituents. These can be expressed in terms of inherent optical properties (IOPs), and apparent optical properties (AOPs). IOPs are those characteristics of the water that are independent of the angular radiance distribution of the light field, and instead, rely on the water medium. Three basic IOPs related to optical remote sensing sensor are absorption coefficient, volume scattering function, and beam attenuation coefficient. In general, optical properties are all wavelength dependent. The beam attenuation coefficient $c(\lambda)$, which is the total light lost from a beam penetrating a water surface, is the sum of scattering $b(\lambda)$, from suspended matters and molecular water, and absorption $a(\lambda)$ of light, by suspended and dissolved matters and water itself. Therefore, the relation of beam attenuation coefficient and other IOPs is as follows (Gordon and Morel 2012; Mobley 1995):

$$c(\lambda) = a(\lambda) + b(\lambda) \qquad (1)$$

AOPs depend on the IOPs and also the angular radiance distribution of the incident light in the water medium. Basic AOP components relative to ORS are irradiance reflectance values and various diffuse attenuation coefficients. The RTE makes a connection between the IOPs and the AOPs (Mobley 1995). Thus, it is the basis for relating remote sensing reflectance (R_{rs}) to concentrations of OAC of water which cause scattering or absorption of light energy. The basic equation RTE is as follows:

$$R_{rs} = G(\lambda) \frac{b_b(\lambda)}{a(\lambda) + b_b(\lambda)} \qquad (2)$$

where

$$a(\lambda) = a_\omega + a_{ph}^*(\lambda)C_{chl-a} + a_{CDOM}(\lambda) + a_{NAP}^*(\lambda)C_{NAP} \qquad (3)$$

$$b_b(\lambda) = 0.5b_\omega(\lambda) + b_{b,ph}^*(\lambda)C_{chl-a} + b_{b,NAP}^*(\lambda)C_{NAP} \qquad (4)$$

where $G(\lambda)$ is the geometrical scaling factor, $a(\lambda)$ is

---

[1]The excessive richness of nutrients in the water, which the water system cannot tolerate.

the total water absorption, Chl-a is the concentration of Chl-a, C_{NAP} is the concentration of NAP, a_ω and $a_{CDOM}(\lambda)$ are the absorptions of water and CDOM, respectively, $a_{ph}^*(\lambda)$ and $a_{NAP}^*(\lambda)$ are the specific absorption coefficients of phytoplankton and non-algal particles, respectively. Also, $b_b(\lambda)$ is the total backscattering coefficient, which similarly is composed of scattering terms for water itself, phytoplankton, and NAP (Kutser et al. 2001; Odermatt et al. 2012). The above two equations are based on the influence of the key water components, including the NAP, pure water, CDOM, and phytoplankton. Initially, most of the bio-optical models for the extracting of water constituents are based on these equations (Olmanson et al. 2015). By giving consideration to that water is often optically complex, a function of any of the three main OAC may overlay one another. Therefore, water types have more requests for instruments with high spatial and spectral resolution, radiometric sensitivity, high accurate atmospheric correction, and water constituent retrieval algorithms (Devred et al. 2013; Matthews 2011).

Remote sensing of Chl-a

In Chl-a studies, satellite remote sensing offers wide regional coverage and high temporal resolution, which are essential for a long period monitoring. Problems have arisen for the Case II waters where total suspended sediments (TSSs) and CDOM have a higher concentration, and their absorptions and scattering do not always have a correlation with phytoplankton, and all components existing in these waters will influence the water optical properties. Therefore, the overlying absorptions by DOM and NAP in the blue part affect the blue-to-green based methods, resulting in unsuitability for measuring Chl-a concentration. This prompted Chl-a retrieval algorithms to emphasize the spectral bands in the red and near-infrared (NIR) spectral regions, which have become common for retrieving Chl-a. These Chl-a retrieval algorithms are parameterized to fit sensor channels. Accordingly, they can frequently be used for estimating Chl-a concentration over the Case-II waters. One of the optical satellites most used for these studies is the Medium Resolution Imaging Spectrometer (MERIS). MERIS had spectral bands situated specifically to measure Chl-a. However, in 2012, this sensor stopped remote transferring data to the Ground. Ocean and Land Color Instrument (OLCI), continuing for MERIS, and Sentinel-2 MSI is current instruments with the potential to conduct Chl-a studies. New satellite products

have to be tested with ground data. Thus, the primary motivation of this study was to examine two current Chl-a retrieval products, fluorescence line height (FLH) and maximum chlorophyll index (MCI), using Sentinel-3 and Sentinel-2.

The European Space Agency (ESA) has developed free, open-source toolboxes for Sentinel-2 and Sentinel-3. Add-in thematic water processing, there are the processors for OLCI and MSI to provide the possible routine enhanced interpretation of water-leaving signals over Case II waters. Two Chl-a-related products, the FLH and MCI, to the sentinel toolbox used to compute the Chl-a fluorescence and scattering peaks by measuring the height of peaks above a specific baseline. The two main objectives of this paper are (1) to test the suitability of these two products for estimating Chl-a concentration with the new sensors in optically complex water and (2) to test the value of Sentinel-2 and Sentinel-3 images with *in situ* measurements and assess the suitability of these sensors to monitor lakes susceptible to intense algal and harmful algae blooms.

Related work

In 1975, after the launch of the Earth Resources Technology Satellites 1 (ERTS-1), Gordon et al. (1988) obtained the first bio-optical model using Monte Carlo simulation of the RTE to build a correlation between AOPs and IOPs. Subsequently, many bio-optical models have been developed for the aquatic system and can be defined in two ways. First, these models can be defined based on the aim of describing the biogeochemical state of the water system. This occurs developing a relationship between radiometric measurements and water constituents to drive information about physical, biological, geochemical processes in the aquatic systems in various ways, which mostly using statistical approaches (Stramski et al. 2001). The second way is based on using RTE to drive quantification of IOPs of OAC of water, then drive the OAC concentration through an analytical approach, for instance, a ratio between their absorption coefficient and specific absorption coefficient or backscattering coefficient to specific backscattering coefficient (Mobley and Sundman 2001).

The light interacting with algae or cyanobacteria can be changed through scattering, fluorescence, and absorption. Bio-optical modeling describes these interactions and obtains information about the optical properties of the phytoplankton and biological characteristics (e.g., size, cellular structure, pigmentation), which govern these changes. Given that

phytoplankton is a microscopic, single cellular organism drifting on the surface water, human eyes or sensors cannot observe it. And in fact, a bulk effect of more than hundreds of cells is what human or remote sensors observe. Therefore, the interaction of bulk cells with light might be described by the theory of single-particle scattering, which is a framework to understand the microscopic level of light interaction with a single cell and present the fundamental theories needed for Chl-a bio-optical modeling. Phytoplankton cells are considerably variable in size, from less than 1 μm to larger than 10 mm. The cells are not only varied by six orders of magnitude in size but can be seen in the form of unicells to a cluster of cells, filaments or colonies. The structure of cells can be different between each phytoplankton species and show different behaviors, for instance, in diatoms silica cell morphology or cyanobacteria gas vacuoles. Despite the diversity in size, form, structure, and behavior that influence the specific optical properties of the phytoplankton, all phytoplankton species contain a green pigment Chl-a. Chl-a is an essential indicator for estimating phytoplankton biomass and lake productivity using Chl-a bio-optical models. These models estimate Chl-a through three pathways: phytoplankton absorption, fluorescence, and backscattering.

Odermatt et al. (2012) provided a comprehensive overview of band arithmetic Chl-a retrieval applications using optical satellites such as SeaWiFS, MODIS, MERIS, Landsat, and HICO to compare various methods and corresponding sensors for Chl-a retrieval methods. Blondeau-Patissier (2014) discussed and compared different algorithms types used for the detection, mapping, and analysis of phytoplankton blooms from various sensors.

Most of the satellite sensors used in water remote sensing operate on sun-synchronous low-orbit satellite platforms. These satellites acquire data with a spatial resolution of a few meters to more than 1 km and temporal resolution of 1–15 days. In the 1970s, passive satellites were first launched to display land and surface water. For example, Landsat Thematic Mapper (TM) was used to retrieve maps of Chl-a, and the results showed that in ideal conditions, the TM could be used with limited accuracy (Dekker 1993). The long-term archive Landsat series over 40 years has been helping to study long-term trends in inland waters. For instance, Landsat ETM[+] was used over 10,000 Minnesota lakes to drive a map of Chl-a, and other water constitutes (Olmanson et al. 2008; Tebbs et al. 2013). Later, the spectral and radiometric sensitivity of sensors, such as NASA's Advanced Land Imager (ALI) and hyperspectral Hyperion sensor, both on the Earth-Observing One (EO-1) satellite, have improved the retrieval of Chl-a (Kutser et al. 2005; Pal et al. 2015).

NASA launched MODIS with an improved spatial resolution of 250–1,000 m for ocean studies, and have used in numerous large-lake studies of Chl-a; that proved the potential of ocean sensors for large-scaled inland waters, despite their relatively coarse spatial coverage, and improved real-time monitoring applications (Wang and Shi 2007). The first two were designed to land, aerosols, and cloud studies, whilst the 1,000 m was designed to watercolor studies. However, some researchers have demonstrated that the 250 and 250 m spatial resolution bands can also be used to monitor algae bloom in inland water bodies (El-Alem et al. 2012; Kahru et al. 2004).

MERIS provides an enhanced spectral resolution and additional key bands that have improved remote sensing of phytoplankton bloom monitoring systems (Matthews et al. 2012; Palmer et al. 2015). MERIS is a push broom system designed to deliver data while the sky is clear or moderately cloudy. This sensor's characteristics are a field of view of 68.5 around nadir with an 1,150 km swath width, 300 m spatial resolution, spectral resolution of 15 bands across the range of 390 nm to 1,040 nm (VIS-NIR), and bandwidth between 2.5 and 30 nm (Binding et al. 2013). Urquhart et al. (2017) applied an assessment approach to quantify changes in the inland cyanoHAB surface area extent using Medium Resolution Imaging Spectrometer (MERIS) imagery across numerous water bodies within Florida, Ohio, and California for the test period of 2008–2012. Their results showed that the area of cyanoHABs in Florida rose significantly due to increased high-risk bloom area while California experienced a slight decline in cyanoHAB extent. In Ohio (excluding Lake Erie), little change in the cyanoHAB surface area was observed. Clark et al. (2017) developed assessment methods to detect cyanoHAB frequency occurrence. Their results showed that 5.6% of waterbodies were resolved by satellites with 300 m resolution, and 0.7% was resolved by applying a 3×3-pixel array based on minimum Euclidian distance from shore. The results also indicate that although land imager such as the Landsat OLI and Sentinel-2 MSI has a higher spatial resolution of 30 m less frequent revisit cycles and less available wavebands for deriving water quality factors. Binding et al. (2018) implemented the spatial and temporal variability analysis of algal blooms on Lake Winnipeg using satellite-derived chlorophyll during 2002–2011.

The results indicated that inter-annual variability in average bloom severity was related to both total phosphorus loadings and summer lake surface temperatures. Nguyen et al. (2019) analyzed the remote sensing images and *in situ* Chl-a data in Lake Kasumigaura, Japan, using available spectral models to achieve optimal Chl-a retrieval. The root-mean-squared (RMS) errors for Chl-a concentration obtained by the resulting model improved from 11.95 mg/m^3 to 6.37 mg/m^3, and the correlation coefficients of Pearson between the predicted and *in situ* Chl-a improved from 0.56 to 0.89. Ledesma et al. (2019) determined the Chl-a distribution and water quality of the Cassaffousth reservoir by developing the statistical models between 2016 and 2017. The regression results represented that Landsat-8 images were related well with field measurements ($R^2 = 0.87$).

Method

In this study, we attempted an assessment, validation, and calibration for analytical research. Although this study is not only a statistical or purely empirical base, we tried to present a semi-empirical base. However, the following sections describe the research procedures.

Study area and dataset

Lake Erie is delimited to the north by Ontario, Michigan to the west, New York to the east, and Ohio and Pennsylvania to the south, and covers a surface area of 25,744 km. Lake Erie is the warmest, shallowest, and most biologically productive of the five Laurentian Great Lakes. It is the fourth largest in the surface area yet smallest in water volume, making it vulnerable to water level fluctuations (Daghighi 2017; Daghighi et al. 2017). This study focuses on the western basin of Lake Erie (see Figure 1). Water depth and nutrient load are the two main factors that impact Chl-a concentration and lead to continuous blooms of green and blue–green algae in this Lake (Maccoux et al. 2016). The western basin is the shallowest section of all the Great Lakes, with an average
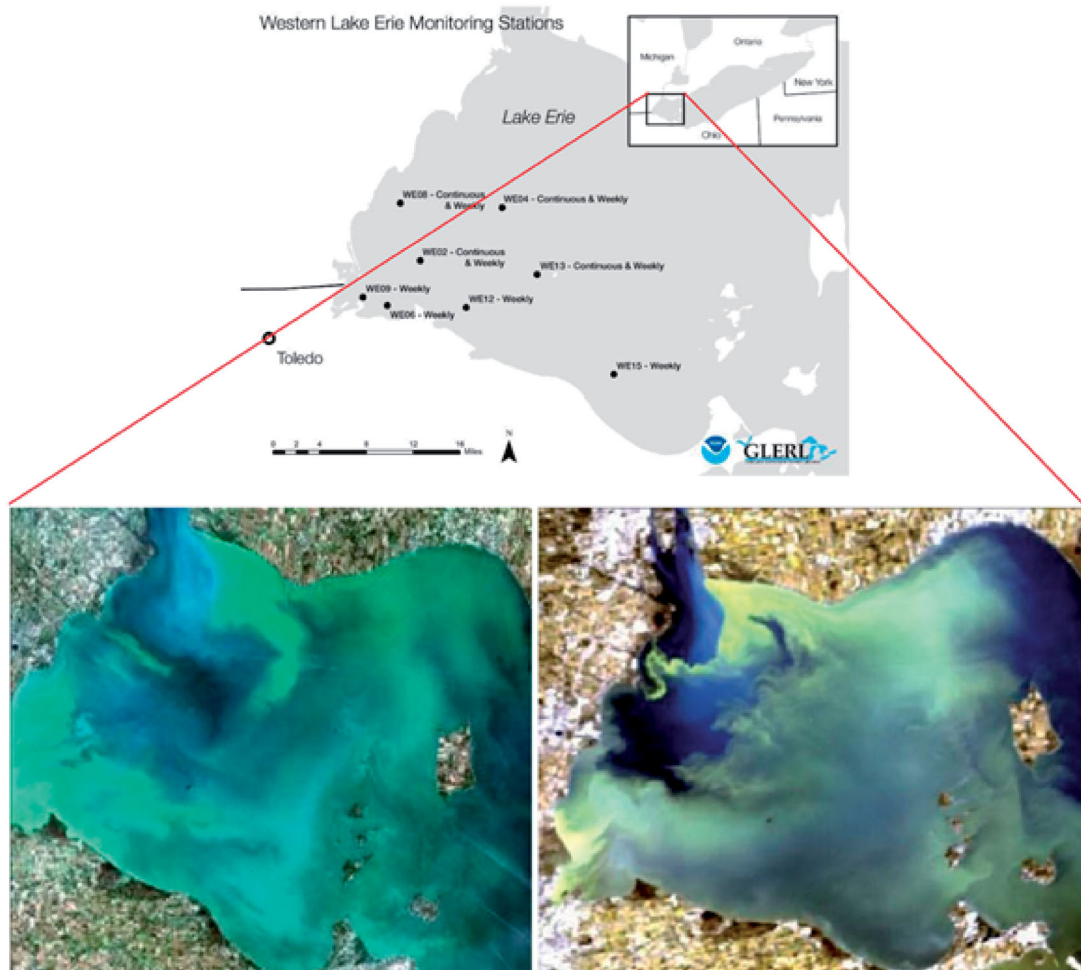
Figure 1. The study area, western Lake Erie. Left: Algal blooms in the lake acquired by Sentinel-2 on October 2, 2017. Right: Sentinel-3 on September 26, 2017.

Table 1. Date of acquisition imagery and water sample acquisition of Sentinel-3A and Sentinel-2A used in this study.

Sentinel-3A		Sentinel-2A	
Filed date	Image date	Filed date	Image date
5/8/2017	5/7/2017	6/26/2017	6/24/2017
5/30/2017	5/30/2017	7/11/2017	7/9/2017
6/12/2017	6/11/2017	7/30/2017	7/29/2017
6/26/2017	6/26/2017	10/2/2017	10/2/2017
7/17/2017	7/16/2017	7/18/2016	7/20/2016
7/31/2017	7/30/2017	8/7/2016	8/9/2016
8/7/2017	8/7/2017	8/29/2016	8/29/2016
8/14/2017	8/14/2017		
8/28/2017	8/26/2017		
9/25/2017	9/26/2017		
10/10/2017	10/8/2017		
10/16/2017	10/16/2017		

depth of 7.4 m, receiving the majority of loaded nutrients, mainly nitrogen and phosphorus. Three main rivers, the Maumee, Raisin, and Detroit Rivers, feed Lake Erie. Although the Detroit River is the primary inlet, contributing up to 90% of the inflow into the lake, the Maumee River loads nearly half of the nutrients into the basin (Charlton et al. 2008). This is because of the Maumee River dominated by agricultural land areas. Compared to the Detroit River (joining Lakes Huron and Erie), which is surrounded by industrial/urban, residential, and partially wood/grassland cover.

We used the weekly Chl-a data measurements from May to October 2017 match with Sentinel-3A, and 2016 and 2017 for Sentinel-2A overpass, respectively. The data were selected to match (3 days window) the image acquisition date. Table 1 shows the image acquisition dates corresponding with filed sampling dates for both Sentinel-2A and Sentinel-3A satellites.

Sentinel-3A OLCI Level-1 NRT FR 2017 images were downloaded from Sentinel-3 Pre-Operations Data Hub (https://scihub.copernicus.eu/s3). Level-1 products provide top of atmosphere (TOA) radiances in the VIS-NIR bands. Twelves Cloud free images were available to match up with the *in situ* data. Sentinel-2 Level-1C images were downloaded from Sentinels Scientific Data Hub. Level-1C products are provided in TOA atmosphere reflectance in cartographic geometry with all parameters to transform them into radiance and the granules (called tiles, $100 \times 100 \, km^2$ ortho-images in UTM/WGS84 projection).

Fluorescence line height (FLH) and base line algorithms

Given that the Chl-a is proportional to the Sun-Induced Fluorescence (SICF) emission, many studies started to examine its validity to measure Chl-a concentration in coastal waters. Results showed a good correlation between Chl-a and SICF (e.g., McKee et al. 2007; Tao et al. 2013). These studies led to the configuration of a few bands on the ocean satellite sensors (such as MODIS, MERIS, GOCI, and OLCI). These bands are positioned slightly differently in each sensor. But, they are all located in the red-edge region, one close to the fluorescence peak and two bands outside of the fluorescence peak, which aim to extract fluorescence radiance through a fluorescence light height (FLH) algorithm (McKee et al. 2007).

In this study, the FLH algorithm estimates the extra reflectance in the fluorescence peak band above a baseline. This baseline connects two reflectance bands positioned outside of the fluorescence peak. This algorithm is identified as follows (Letelier and Abbott 1996):

$$\text{FLH} = L2 - \left[L3 + \frac{(L1 - L3)(\lambda 3 - \lambda 1)}{\lambda 3 - \lambda 1} \right] \quad (5)$$

where $L1$, $L2$, and $L3$ are radiances at wavelengths $\lambda 1$, $\lambda 2$, and $\lambda 3$, respectively. The FLH algorithm is more accurate when used for case I and oligotrophic waters. This is because the atmospheric correction works better for ocean waters, and also the elastic scattering signals are low above the baseline curve. Recently, in inland waters, with the improvement of atmospheric algorithms, turbidity is the main source of reducing the sensitivity of the FLH algorithm. The reflectance peak around 700 nm influences the fluorescence peak around 685 nm retrieval. This reflectance peak is related to increased water absorption, decreased Chl-absorption, increased particulate backscattering in this spectrum region. Despite CDOM absorptions ($\sim$440 nm) having a low effect on FLH signals, suspended sediments ($5 \, gm^{-3}$) result in a significant error due to the particulate scattering. Moreover, FLH application in high phytoplankton biomass ($>$20 mg/m^3) (Tao et al. 2013) is hindered by a peak reflectance overlapping the fluorescence reflectance. This peak shifts to the longer wavelengths with increasing Chl-a concentration (e.g., to 705 nm at 100 mg/m^3). Therefore, the FLH algorithm is more applicable for oligo to mesotrophic waters less than 20 mg m^{-3} used in this study (Gitelson 1992).

In addition, we used the Baseline algorithm, which exploits the height of the fluorescence and maximum scattering peak of Chl-a above a baseline, which passes through two other spectral bands outside of the peak. The general equation of a baseline algorithm is the line-height:

$$\text{Line height} = L2 - L1 - (L3 - L1)\left[\frac{(\lambda 2 - \lambda 1)}{\lambda 3 - \lambda 1}\right] \tag{6}$$

where indices 1 and 3 indicate the baseline bands and index 2, the peak or signal band. This algorithm used by Gower et al. (2003) and was characterized by MERIS toolbox. However, the algorithm applied in the FLH/MCI processor in the Sentinel Application Platform (SNAP) contains an additional factor to correct the influence of thin clouds using $K = 1.005$:

$$\text{Line height} = L2 - K$$
$$\times \left[L1 + (L3 - L1)\frac{(\lambda 2 - \lambda 1)}{\lambda 3 - \lambda 1}\right] \tag{7}$$

Image processing

Sentinel-3 Toolbox (S3TBX) version 6.0.0 in the Sentinel Application Platform (SNAP) on Windows 10 (64 bit) was used to process the images. Images were subset to a geographic region bounded by the latitude and longitude to limit the lake of interest. The conversion from TOA radiance (LTOA) to TOA reflectance (RTOA) was done in SNAP Data Processors to be further analyzed. The conversion from TOA radiance (LTOA) to TOA reflectance (RTOA) has been done through SNAP Data Processors-Radiance-to-Reflectance Processor. This conversion aims to extract the pixel Level-1B data and convert the included radiance into reflectance through three main steps: first, pre-processing for geometry and meteorological parameters (i.e., pressure, wind) at each pixel. Second, pixel identification starts with the reading of the INVALID flag. If it is set to TRUE, no further processing of the current pixel is performed, and the next pixel is examined. Otherwise, the processing of the current pixel is pursued. Third, pixel extraction and reflectance conversion.

Thematic water processing using FLH/MCI Processor was performed to extract MERISFLH and MERISMCI signals. The FLH/MCI processor can be invoked in the Sentinel Toolbox from the tool menu by selecting Processing Thematic Water Processing, FLH/MCI Processor. We defined a new red-edge peak height band combination, by the Processor and named it S3FLH. We were able to develop this new algorithm because, in the FLH/MCI processor, the baseline bands and the signal band are freely configurable. Two different signal bands, 709 nm and 681 nm,

with varying bands of baseline (665, 673, and 753 nm) were configured to calculate MERISFLH, MERISMCI, and S3FLH. Level-1 MCI/FLH products are calculated from the TOA radiance, which has the units of $mWm^{-2}\ nm^{-1}\ sr^{-1,}$ whereas the L2 MCI/FLH products are derived from water-leaving reflectance, which is dimensionless.

Cloud-free pixel values corresponding to the location of each sampling station were extracted from each thematic product to be evaluated with the ground data. To extract the MCI and FLH indices from the images at locations specified in a point feature class, we used the Extract Multi Values to Points tool with ArcGIS. Each pixel which covered the geographic location of the station value extracted for each input raster, and a new field containing the cell values for each input raster added to the input point feature class. Then an attribute table exported to Microsoft Excel to establish a relationship between the radiometric indices and *in situ* Chl-a content and assessment of created models. Figure 2 shows an overview of the method applied in this study.

Sentinel-2 Toolbox (S2TBX) Version 6.0.0 in the Sentinel Application Platform (SNAP) on Windows 10 (64 bit) was used to process the images. Sentinel-2 is delivered with three spatial resolution options. The spatial resolution of Sentinel-2 is dependent on the particular spectral band. Level1C Sentinel-2 data includes the RGB-NIR as 10 m bands and SWIR as 20 m bands. As the SNAP feature is not supported for a multi-size product, we needed to upscale the RGB-NIR bands to 20 m and resample them with the rest of the 20 m bands. The spatial subset of data created by given pixel positions using a subset operator. Sentinel-2 MCI Processor was used to calculate the MCI, which calculates the MCI by exploiting the height of a measurement over a specific baseline. We configured the suited band combination on Sentinel-2 MSI images (a signal band at 705 nm above the baseline passing through 665 and 740 nm bands) to exploit the height of a maximum Chl-a peak. Pixel values were extracted from each sampling location to correlate with *in situ* Chl-a measurements. To extract the indices from raster images to a table, we used ArcGIS spatial analysis tools by extracting the values of each pixel, which covered the geographical location of the station value and then registering the values in an attribute table of a predefined point layer. Finally, a CSV-file format exported as an output to establish a model between the extracted indices and Chl-a contents.
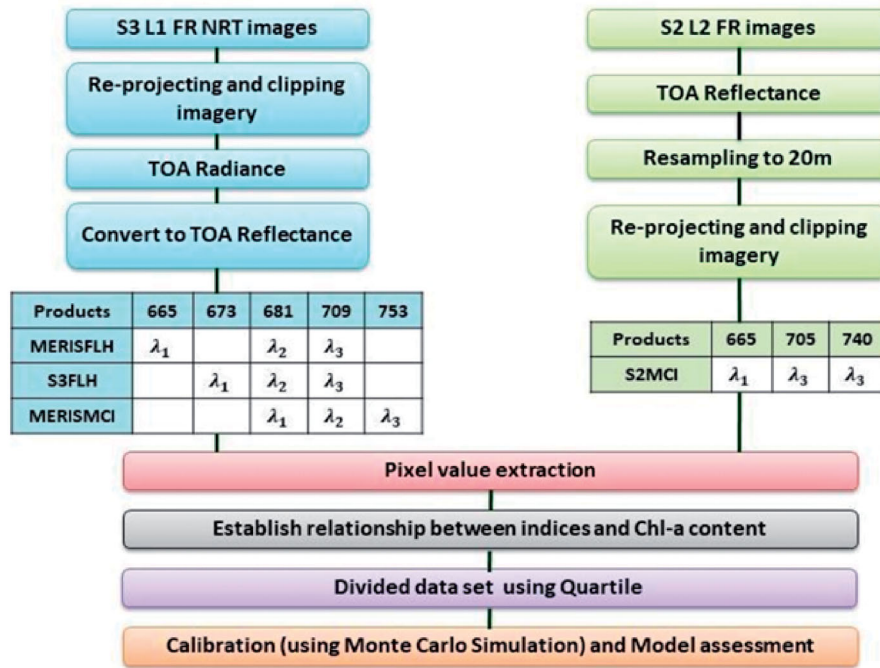
Figure 2. Processing flowchart of Sentinel-3A OLCI and Sentinel-2A MCI images to retrieve Chl-a indices related to *in situ* Chl-a Concentration.
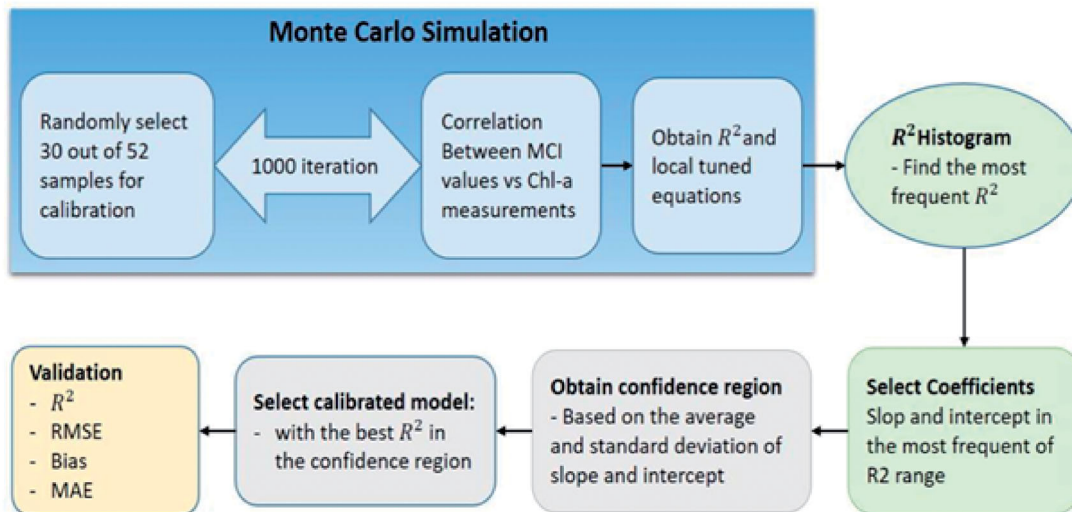

Figure 3. Monte Carlo calibration and validation scheme.

Calibration and validation

Monte Carlo simulation in MATLAB was used to calibrate the models (Figure 3). Monte Carlo simulation is a technique used to study how a model responds to randomly generated inputs. In this process, 30 samples randomly selected from the dataset of 52 are used to build the equations with a linear regression between Chl-a and the product retrieval values iterating 1,000 times. The results are recorded for 1,000 equations and R^2, slope, and intercept associated with each. Then an R^2 histogram created from all the

recorded R^2 to identify equations with the most frequent range of this coefficient. We plot the coefficients (slope, intercept) of the identified equations to obtain a confidence region. The calibrated model was selected with the best R^2 in the confidence region based on mean and standard deviation. Then we validated the equation with 22 test data.

The same calibration and validation process were carried out for the S2MCI indices and match up *in situ* dataset generated. In the process, 15 samples randomly selected from the dataset of 27 are used to

build the equations with a linear regression between Chl-a and the product retrieval values iterating 1,000 times. The results are recorded for 1,000 equations and R^2, slope, and intercept associated with each. Then an R^2 histogram created to obtain the most frequent R^2 from all the recorded R^2 to identify equations with the most frequent range of this parameter.

Results and discussion

Chl-a measurement from Sentinel-2

Table 2a illustrates the basic descriptive statistics of Chl-a measurements and confirms the complexity of optical properties of the waters being measured in western Lake Erie over summer 2017. N is the number of samples collected, and Std is the standard deviation. In this study, the three models were evaluated for Chl-a less than 300 mg/m³ with a range of 1.28–116 mg/m³ with a mean value of 19.66 mg/m³. Figure 4 depicts the monthly variation of all weekly Chl-a measurements. The dataset is representative of a broad range of Chl-a concentrations. Overall, the level of Chl-a increases gradually over the months, showing the lowest values in May and the highest in August and September.

Table 2b shows the summary of basic descriptive statistics of measured Chl-a concentration of the waters being measured on 24 June, 9 and 29 July, 2
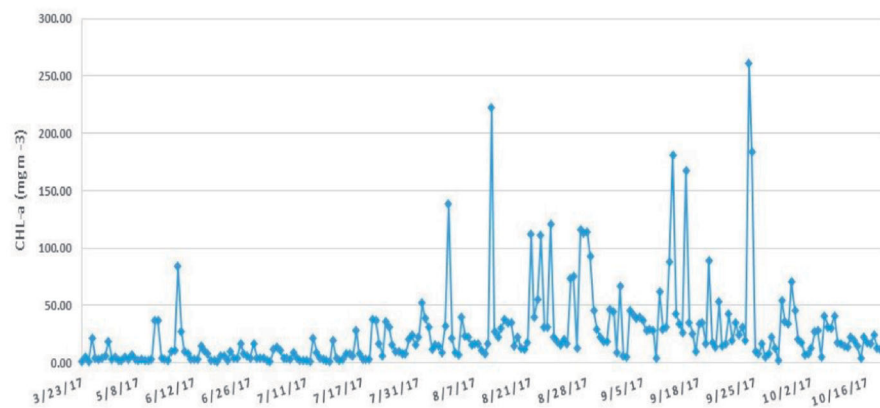
October in 2017 and 18 July, 9 and 29 August 2016 in Western Lake Erie match up with the Sentinel-2 image acquisition dates. In this study, we evaluated the L2 S2MCI product for the data with a range of 0.13 to 88 mg/m³ with a mean value of 16.5 mg/m³.

### Chl-a measurement from Sentinel-3

We used *in situ* Chl-a measurements to analyze the performance of FLH and MCI algorithms based on Sentinel-3 spectral bands. Figures 5 and 6 show the retrieval of the fluorescence and scattering components from the Sentinel-3 images correlated with Chl-a and log Chl-a. Three bands are utilized for each of the three algorithms to compute FLH and MCI. The bands are 665, 681, and 709 nm for MERISFLH (Gower et al. 1999) and 681, 709, and 753 nm for MERISMCI (Gower et al. 2005). An additional Sentinel-3 band exists at 673 nm; thus, we configured 673, 681, and 709 nm and named it S3FLH algorithm. Tables 3a and 3b present local tuned equations, R^2, and RMSE for the three Sentinel-3 products. Figure 7 shows the correlation between FLH and MCI indices and Log Chl-a in a range of 10–120 mg/m³.

Comparing Sentinel-2, Sentinel-3 and *in situ*

We compared both images and *in situ* data to determine the performance of the Chl-a model. The result of FLH and MCI products in Level-2 processing, which is the normalized FLH and MCI, shows lower performance compared to the processing of Level-1 products. This normalization included pre-processing of geometrical and meteorological parameters (such as wind and pressure, bidirectional effects) at each pixel, pixel screening to find the valid pixel and conversion of the radiance signal to reflectance. The lower performance of normalized FLH and MCI radiances

Table 2. (a) Descriptive statistics of Chl-a measurements match up with Sentinel-3 satellite overpass acquisition times for western Lake Erie over summer 2017; (b) Descriptive statistics of Chl-a measurements match up with Sentinel-2 satellite overpass acquisition times for western Lake Erie over the summer 2016 and 2017.

		N	Min	Max	Mean	Median	Std
(a)	Chl-a (Sentinel-3)	74	1.28	116	19.66	14.8	22.16
(b)	Chl-a (Sentinel-2)	37	0.13	88	16.5	9.2	20.7

Unit is mg m³.

**Figure 4.** Time series of measured Chl-a obtained from NOAA-GLERL (May to October 2017).
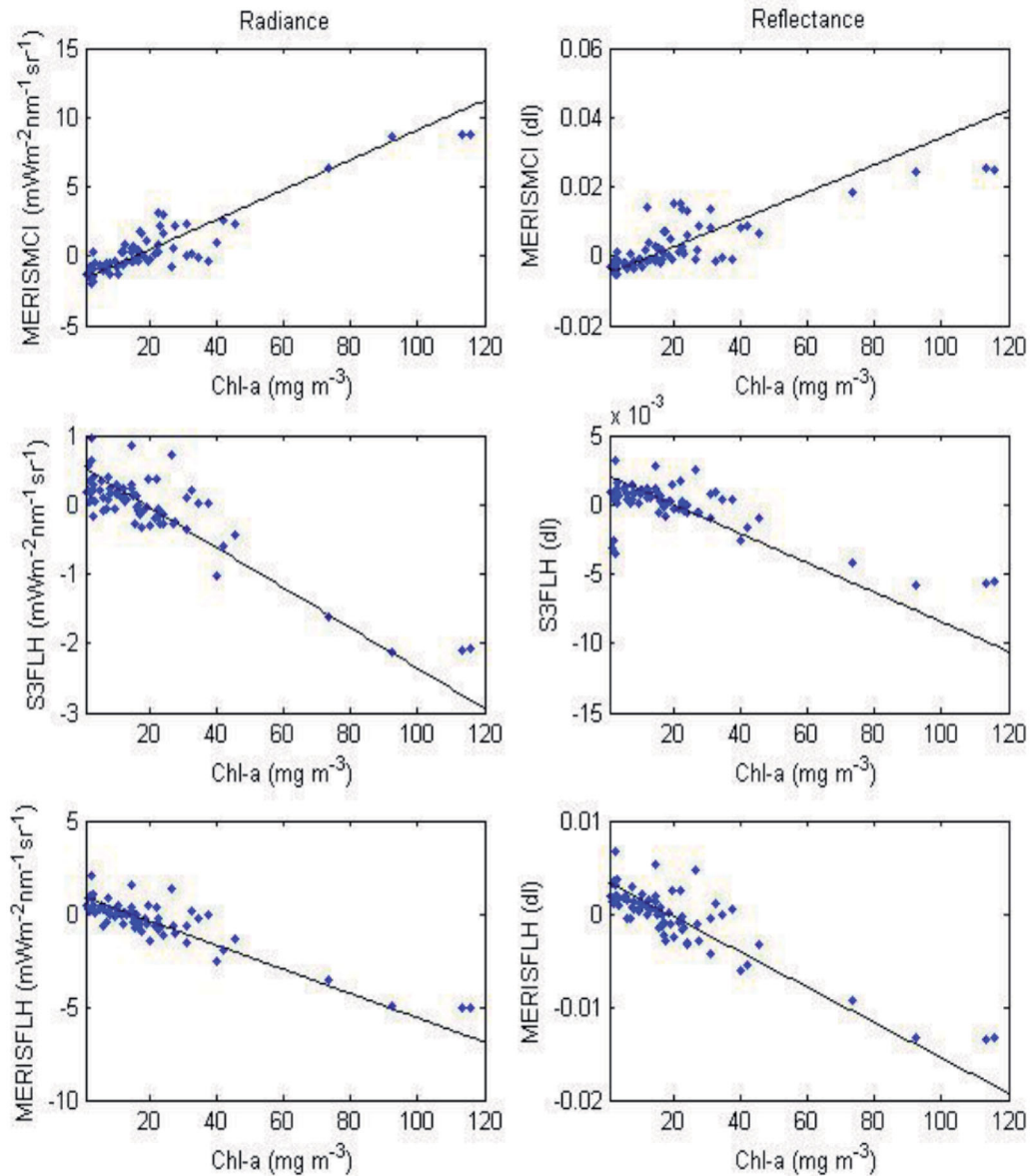
Figure 5. Correlation between FLH and MCI indices and *in situ* Chl-a using Sentinel-3 bands in TOA radiance and TOA reflectance.

might be related to the poor pixel identification during the process of pixel flagging, which is affected by the complexity of the water and atmosphere condition.

MERISFLH accomplishment

MERISFLH using 665, 681, and 754 nm performed better in comparison to the band combination of 673, 681, and 754 nm (S3FLH), respectively. This finding might be related to the closer positioned 673 nm proximate to 681 nm, which makes the baseline a less accurate replacement of the elastic radiance (with the baseline) compared to the other band combinations. This sensitivity of the proximity of the band selection for FLH products in Case II, waters are not seen in

the Case I waters due to the low water constituents' influences on the elastic radiance reflectance in the red spectral region. Nevertheless, despite their correlation of $R^2 = 0.79$; 0.76 in both algorithms, MERISFLH and S3FLH, respectively, the results could be biased and not applicable for the lake type studied. As shown in Figure 5 for the FLH band configurations, the FLH is positively correlated with Chl-a values up to $8 \, \text{mg/m}^3$. However, at the higher Chl-a concentration, the FLH values become rapidly negative. This behavior is strongly due to the shift of the reflectance peak to the longer wavelengths along with the increase in [Chl-a] values (Gitelson et al. 2009). FLH algorithms have proven to be applicable to the ocean and oligotrophic waters, where the Chl-a
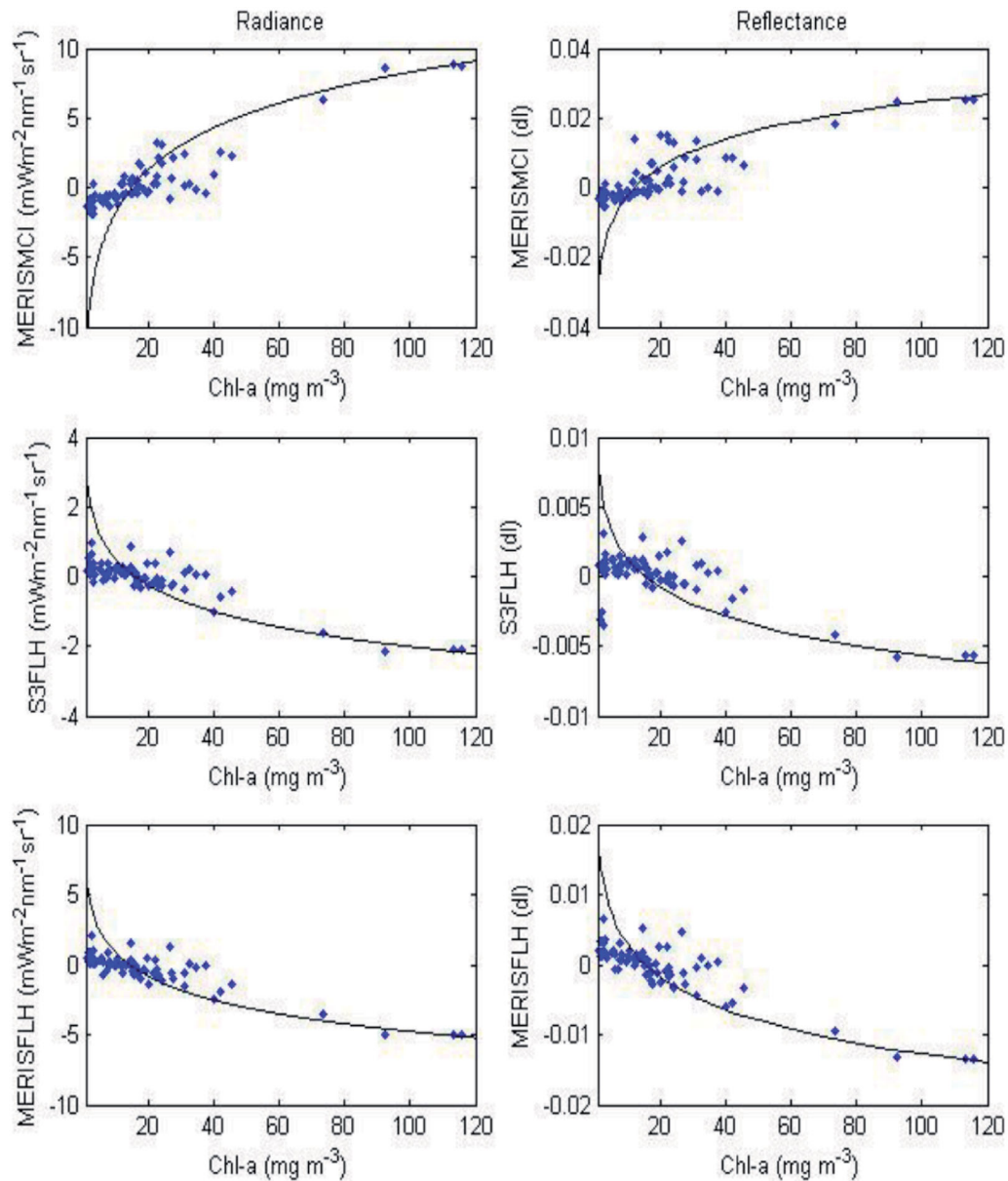
Figure 6. Correlation between FLH and MCI indices and log Chl-a using Sentinel-3 bands in TOA radiance and TOA reflectance.

concentration is less than $10 \, \text{mg/m}^3$. This limitation is due to the replacement of elastic reflectance to the baseline between $\lambda 1$ and $\lambda 2$, which deviate (associated with the cell scattering) from the flat line with increasing Chl-a amounts. However, in the low Chl-a concentrations, the baseline nearly matches the elastic reflectance in the red region.

MERISMCI accomplishment

MERISMCI products have been shown as a useful tool for monitoring algal blooms in optically complex water. In this paper, with a [Chl-a] range $0.1–300 \, \text{mg/m}^3$, this product presented the best performance for both L1 and L2 products processed compared to FLH

products. The retrieved MCI showed a strong linear correlation with the Chl-a measurements (Chl-a = 8.9 MERISMCI + 15.98, R^2 =0.82, and RMSE = 8.86). Binding et al. (2011) investigated a comprehensive evaluation of all Chl-a MERIS products and determined the MCI to be a more effective algorithm for eutrophic conditions. They also studied the assessment of MCI for waters ranging from optically complex to low Chl-a conditions. Their results showed the MCI algorithm to be a useful tool in algae monitoring with Chl-a range of $10–300 \, \text{mg/m}^3$ (Binding et al. 2013).

In our study, also in agreement with Binding et al. (2011) and Binding et al. (2013), the MCI values are negative or negligible for almost Chl-a $< 20 \, \text{mg/m}^3$,

Table 3. (a) Equations and performance of the Chl-a model for Sentinel-3A; (b) Equations and performance of the Log Chl-a model for Sentinel-3A; (c) Equations and performance of Log Chl-a (10–120 mg/m^3) model for Sentinel-3A.

Model	Locally tuned equation	R^2	RMSE
(a)			
MERISMCI Rad.	Chl-a $= 8.9$ MCI $+ 15.98$	0.82	8.86
S3FLH Rad.	Chl-a $= -34.6$ MCI $+ 18.3$	0.76	10.8
MERISFLH Rad.	Chl-a $= -15.4$ FLH $+ 13.8$	0.79	10.1
MERISMCI Ref.	Chl-a $= 2548$ MCI $+ 13.3$	0.67	12.7
S3FLH Ref.	Chl-a $= -9464$ MCI $+ 20$	0.54	15
MERISFLH Ref.	Chl-a $= -5292$ FLH $+ 18$	0.77	10.5
(b)			
MERISMCI Rad.	MCI $= 4.38$ log(Chl-a) $- 11.9$	0.83	8.4
MERISMCI Ref.	MCI $= 0.01$ log(Chl-a) $- 0.02$	0.76	10.1
S3FLH Rad.	FLH $= -1.08$ log(Chl-a) $+ 3.0$	0.81	9.01
S3FLH Ref.	FLH $= -0.003$ log(Chl-a) $+ 0.008$	0.67	12.3
MERISFLH Rad.	FLH $= -2.42$ log(Chl-a) $+ 6.41$	0.82	8.5
MERISFLH Ref.	FLH $= -0.007$ log(Chl-a) $+ 0.02$	0.8	8.5
(c)			
MERISMCI Rad.	MCI $= 5.24$ log(Chl-a) $- 15.8$	0.87	8.4
MERISMCI Ref.	MCI $= 0.014$ log(Chl-a) $- 0.038$	0.76	11.8
S3FLH Rad.	FLH $= -1.33$ log(Chl-a) $+ 4.09$	0.87	8.1
S3FLH Ref.	FLH $= -0.004$ log(Chl-a) $+ 0.012$	0.87	8.2
MERISFLH Rad.	FLH $= -2.88$ log(Chl-a) $+ 8.49$	0.88	7.8
MERISFLH Ref.	FLH $= -0.008$ log(Chl-a) $+ 0.024$	0.87	8.1

meaning that there was no reflectance in the peak 709 nm, the peak should be shifted to the shorter wavelengths for could capture by FLH products at 681 nm. Moses et al. (2009) suggest the threshold of 10 mg/m^3 for MCI application. Gower et al. (2008) noted the applicability of the MCI algorithm for Chl-a concentration above 30 mg/m^3. We tuned the equation for Chl-a values > 30 mg/m^3. Subsequently, the MCI showed a strong correlation with $R^2 > 0.91$. L2S2MCI, with the combination of 665, 705, and 740 nm to compute the MCI from the Sentinel-2 images, showed a very good correlation with the *in situ* Chl-a data in the studied stations (Chl-a $= 2158$ S2MCI $+ 3.9$, $R^2 = 0.92$, and RMSE $= 6.03$).

Moreover, the calibrated model was selected with the best R^2 in the confidence region based on mean and standard deviation. Then we validate the equation with 10 test data. Figure 8 illustrates histograms of the R^2 distribution for MERISMCI and S2MCI algorithms. Figure 9 also shows plot of the slope versus intercept.

S2MCI accomplishment
Figure 10 displays the correlation between S2MCI and *in situ* Chl-a. The sensor has the advantage of higher spatial resolution (10 and 20 m) compared to Sentinel-3 OLCI instruments (300 m), which make it useful for monitoring small lakes (Toming et al. 2016). Water constituents are varied spatially even within a few meters and within a short period; for instance, during the raining season, loading a mass of particulate and dissolved matters discharge into the water body. Kutser (2004) studied the extent of blue–green algae

using different satellite sensors. The result noted the limitation of these sensor spatial resolutions for quantitatively accurate estimation of the Chl-a, as the high variation in the phytoplankton biomass happens at smaller than 30 m scales.

This study shows that the results of S2MCI have the potential to improve with an advanced atmospheric correction. Inland waters have the limitation of enhanced atmospheric correction algorithms compared to the ocean water. Toming et al. (2016) used Sen2cor in the Sentinel-2 toolbox for atmospheric correction of Sentinel-2 Level-1 data in mapping Chl-a. However, their results showed a lower correlation between algorithm values versus field measurements. In contrast, this study showed that retrieving the scattering peak around the red-edge region while applying the developed atmospheric corrections has ineffective results spatially in the blue–green bloom observations. Sentinel-3 OLCI images were atmospherically corrected using the Case-2 Regional/Coast Color (C2RCC) tool in the SNAP Sentinel-3 toolbox to measure the MCI during the algae bloom. The comparison of TOA radiance and BOA reflectance showed poor performance of C2RCC in the bloom condition (Toming et al. 2017). Nevertheless, the red-edge band algorithms are relatively less influenced by the atmospheric effects, which is a greater advantage of using this spectral region compared to blue–green algorithms that use the blue–green region.

MERISMCI and S2MCI calibration and assessment of performance are presented in Table 4 for Chl-a estimation in western Lake Erie, with the statistical performance estimators. We also plotted the estimated Chl-a values of Sentinel-2 and Sentinel-3 retrieval MCI correlated with the Chl-a measured values to see the 1:1 model estimation performance. We split the extreme data and show the remaining data in the plots displaying in Figure 11. The results indicate no significant differences between the retrieval algorithms in comparison with the *in situ* measurements, Sentinel-2 ($R^2 = 0.92$, 0.84, RMSE $= 6.03$, 9.6) and Sentinel-3 ($R^2 = 0.83$, 0.86, RMSE $= 8.59$, 8.61) (Table 4) for calibration and validation, respectively. However, the inaccurate estimation will be inevitable using all Chl-a concentration ranges affected by deviating the peak along with Chl-a content variation (Augusto-Silva et al. 2014).

In this study, the result for Sentinel-2 MCI showed better performance ($R^2 = 0.92$). This finding is highly related to the 300 m spatial resolution of OLCI pixel values. It is one of the significant problems of ocean satellite application to lake studies with substantial
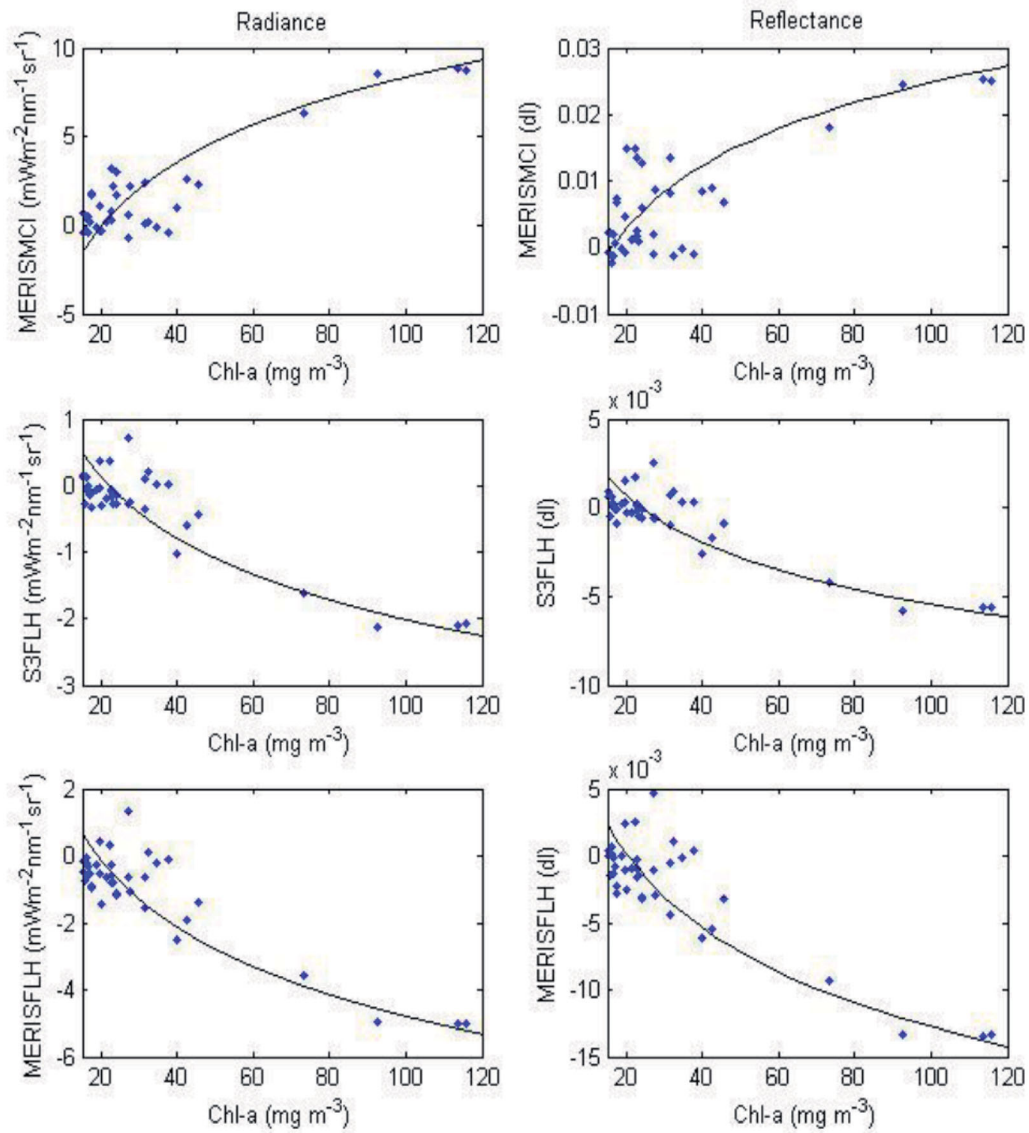
Figure 7. Correlation between FLH and MCI indices and log Chl-a (10–120 mg/m³) using Sentinel-3 bands in TOA radiance and TOA reflectance.
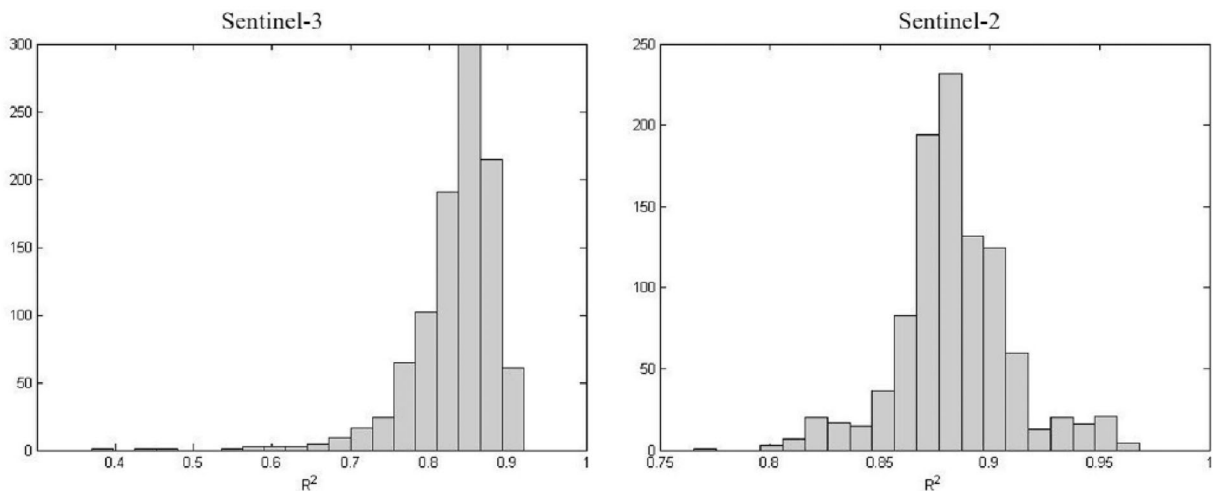
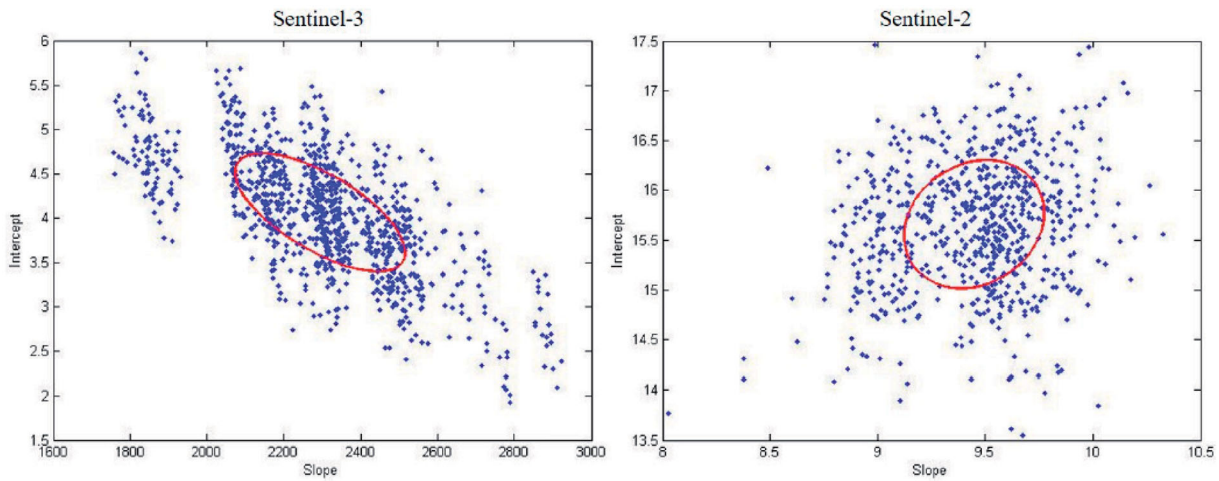**Figure 8.** Histograms of the R^2 distribution for MERISMCI and S2MCI algorithms.
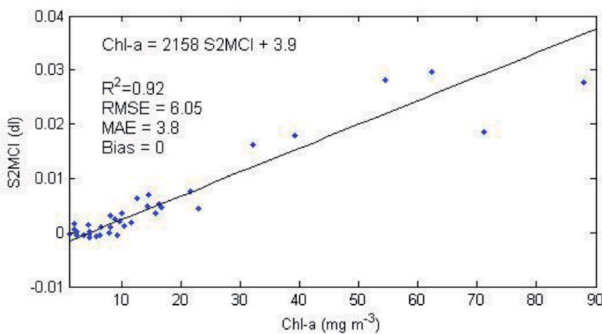
Figure 9. Plot of the slope vs intercept.

Figure 10. Correlation between S2MCI and *in situ* Chl-a.

Table 4. Performance of the calibration and validation algorithms.

Algorithm	Calibration				Validation			
	R^2	RMSE	MAE	Bias	R^2	RMSE	MAE	Bias
MERISMCI Rad.	0.83	8.59	6.64	0	0.86	8.61	6.01	−1.3
S2MCI Ref.	0.92	6.05	3.8	0	0.84	9.6	6.66	0.15

optical property variations in meter scales. Both instrument applications will benefit from an advanced atmospheric correction. The MCI has been shown to be negligibly affected by the CDOM due to the spectral distance of the red-edge peak from the blue wavelength. In Lake Erie, that the suspended sediment is a major contribution to the optical signal, increasing the magnitude of spectral reflectance, likely is the significant source of error in MCI approaches (Augusto-Silva et al. 2014). The use of MCI in shallow waters may be affected by the seagrasses and sandy bottom, which contribute to peak reflectance in the red-edge region (Hill et al. 2014). To have a more accurate evaluation, we needed more *in situ* parameter measurements with fuller information about their quality, and accuracy of measuring instruments in field and

laboratory since these highly affect satellite product performances and evaluation.

Conclusions

In this study, we have assessed four Chl-a retrieval products. For two of the products (MERISFLH and MERISMCI) already characterized to fit MERIS bands, we configured a new algorithm (S3MCI) based on Sentinel-3 band combination and Sentinel-2 S2MCI product to retrieve Chl-a concentration. We used the Chl-a data from western Lake Erie weekly monitoring stations. We concluded that the different Chl-a range limitations for the MCI products can be due to the different locations of the maximum peak bands, 705 nm and 709 nm for MSI and OLCI sensors, respectively.

This study suggested that the application of Sentinel-2 and Sentinel-3 data to estimate phytoplankton Chl-a concentrations in the Western Basin of Lake Erie perhaps is a good method to test it in other geographical regions. We concluded the highlights and the contribution of this study as (i) evaluating the potential of Sentinel-3 Ocean and Land Color Instrument (OLCI) and Sentinel-2 Multispectral Instrument (MSI) data, (ii) testing Chl-a-related products by using NOAA-Great Lakes Chl-a monitoring data over summer 2016 and 2017; (iii) fluorescent light height (FLH) algorithms are limited to lakes with Chl-a < 8 mg/m³, and (iv) sentinel-3 MCI is suggested for Chl-a > 20 mg/m³ and Sentinel-2 MCI for Chl-a > 8 mg/m³. Our finding suggests that Sentinel-2 MCI achieved better performance for Chl-a retrieval (R^2 = 0.92) than the existing methods. Perhaps, this study can be a good contribution to environmental studies
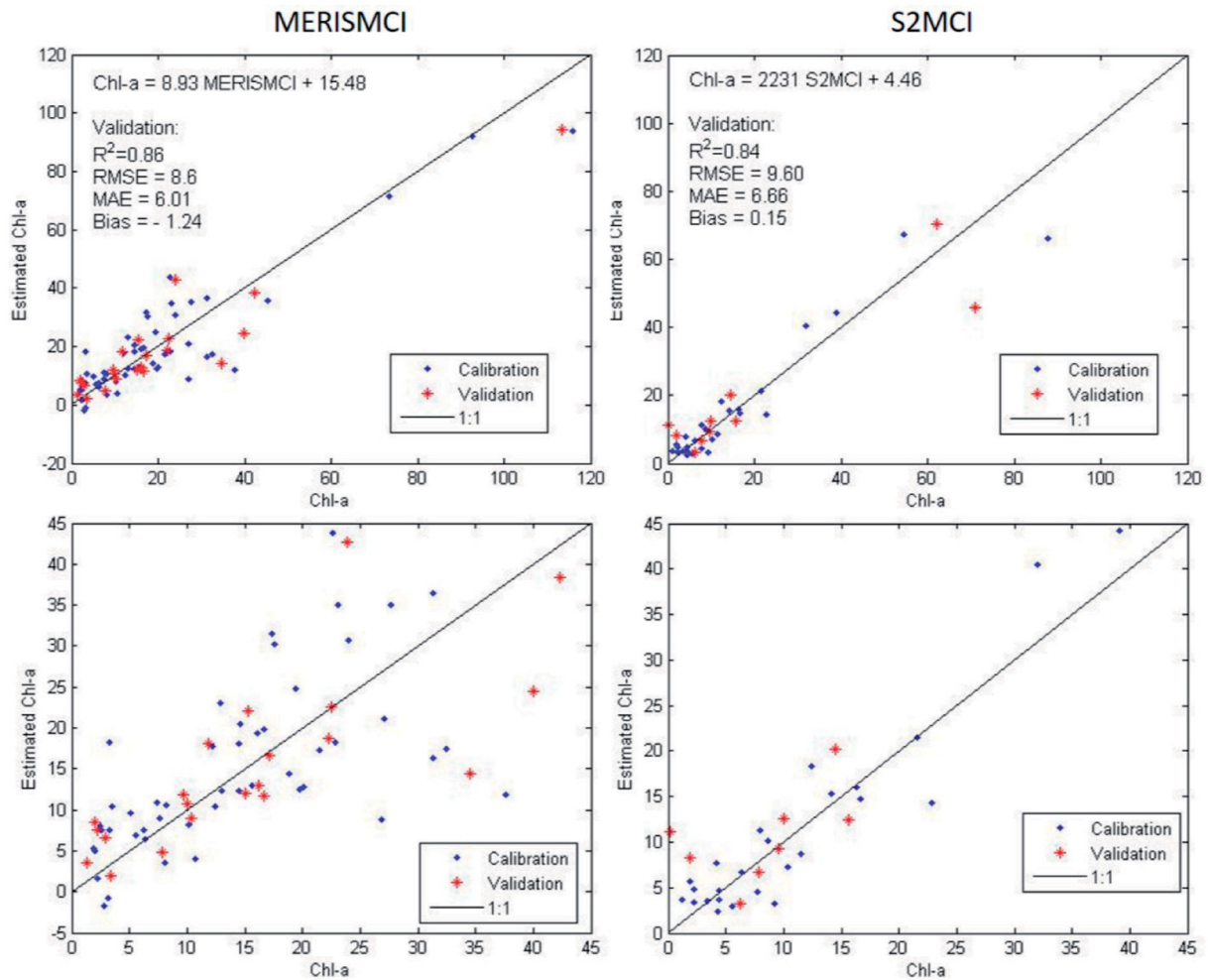
Figure 11. Estimated Chl-a vs *in situ* Chl-a, calibration and validation dataset.

and researchers in the future who may work on Phytoplankton Chl-a concentrations Sentinel data.

In contrast, the MCI approach is limited to Chl-a retrieval above $20 \, mg/m^3$. However, FLH and MCI approach both have the advantages of being less influenced by atmospheric effects. Sentinel-2 MCI product offered the highest performance in this study. This performance is mainly related to the high spatial resolution of the MSI sensor, which is a necessity of sensor characterization in Chl-a estimation. Furthermore, the performance is due to the maximum peak location of 705 nm in the S2MCI band combination compared to 709 nm of the MERISMCI signal band position. This study indicates the suitability of Sentinel-3 and Sentinel-2 satellite products using the red-edge scattering approaches for use in monitoring phytoplankton biomass (in large Chl-a range values) with a highly promising result to add services aimed at reducing the impact of the eutrophication on aquatic systems.

Future works

This study demonstrated the potential of the MCI algorithms to monitor green algae blooms in eutrophic lakes qualitatively. However, there is still some inconsistency between *in situ* Chl-a measurements and MCI that currently precludes their application as a robust quantitative approach for estimating the bloom condition. This is mainly due to the high variability of the regional and temporal optical properties of the water bodies. Moreover, diverse phytoplankton taxonomy with different pigment composition, cell size, population distribution, and the display of species behaviors in different environmental conditions are mainly in the case of cyanobacteria. They are profoundly impacted by spectral reactance due to their vertical distribution in the water column (Kutser et al. 2005). Therefore, we suggest considering variable IOPs in developing bloom monitoring algorithms in addition to finding the depth of

phytoplankton *in situ* samplings for model assessment would enhance bloom studies in the future studies. The authors suggest that this study would be improved by creating Chl-a mapping by the different processors, which could help show the performance of each product in displaying the extent of bloom and information about the spatial distribution of Chl-a concentrations.

Disclosure statement

No potential conflict of interest was reported by the author(s).

ORCID

Saied Pirasteh http://orcid.org/0000-0002-3177-037X
Sarah Narges Fatholahi http://orcid.org/0000-0001-9757-6783
Jonathan Li http://orcid.org/0000-0001-7899-0049

Data availability statement

Data and code are available upon request.

References

Amanollahi, J., Ahmad, M.A., Ramli, M.F., and Pirasteh, S. 2012. "Influences of the window size of moderate resolution imaging spectroradiometer (MODIS) aerosol optical thickness (AOT) values on particulate matter (PM10) motoring in Klang Valley, Malaysia." *Scientific Research and Essays*, Vol. 7(No. 12): pp. 1373–1380. doi:10.5897/SRE12.040.

Augusto-Silva, P.B., Ogashawara, I., Barbosa, C.C., De Carvalho, L.A., Jorge, D.S., Fornari, C.I., and Stech, J.L. 2014. "Analysis of MERIS reflectance algorithms for estimating chlorophyll-a concentration in a Brazilian reservoir." *Remote Sensing*, Vol. 6(No. 12): pp. 11689–11707. doi:10.3390/rs61211689.

Binding, C., Greenberg, T., and Bukata, R. 2013. "The MERIS maximum chlorophyll index; its merits and limitations for inland water algal bloom monitoring." *Journal of Great Lakes Research*, Vol. 39: pp. 100–107. doi:10.1016/j.jglr.2013.04.005.

Binding, C., Greenberg, T., Jerome, J., Bukata, R., and Letourneau, G. 2011. "An assessment of MERIS algal products during an intense bloom in Lake of the Woods." *Journal of Plankton Research*, Vol. 33(No. 5): pp. 793–806. doi:10.1093/plankt/fbq133.

Binding, C., Greenberg, T., McCullough, G., Watson, S.B., and Page, E. 2018. "An analysis of satellite-derived chlorophyll and algal bloom indices on Lake Winnipeg." *Journal of Great Lakes Research*, Vol. 44(No. 3): pp. 436–446. doi:10.1016/j.jglr.2018.04.001.

Blondeau-Patissier, D., Gower, J.F., Dekker, A.G., Phinn, S.R., and Brando, V.E. 2014. "A review of ocean color remote sensing methods and statistical techniques for the detection, mapping and analysis of phytoplankton blooms in coastal and open oceans." *Progress in Oceanography*, Vol. 123: pp. 123–144. doi:10.1016/j.pocean.2013.12.008.

Charlton, M., Vincent, J., Marvin, C., and Ciborowski, J. 2008. "Status of nutrients in the Lake Erie basin." US EPA. Accessed 20 April 2020. https://www.epa.gov/sites/production/files/2015-10/documents/status-nutrients-lake-erie-basin-2010-42pp.pdf.

Clark, J.M., Schaeffer, B.A., Darling, J.A., Urquhart, E.A., Johnston, J.M., Ignatius, A., Myer, M.H., Loftin, K.A., Werdell, P.J., and Stumpf, R.P. 2017. "Satellite monitoring of cyanobacterial harmful algal bloom frequency in recreational waters and drinking source waters." *Ecological Indicators*, Vol. 80: pp.: 84–95. doi:10.1016/j.ecolind.2017.04.046.

Daghighi, A. 2017. *Harmful algae bloom prediction model for western Lake Erie using stepwise multiple regression and genetic programming*. MSc Thesis. Cleveland: Cleveland State University. Accessed 20 April 2020 https://engagedscholarship.csuohio.edu/etdarchive/964

Daghighi, A., Nahvi, A., and Kim, U. 2017. "Optimal cultivation pattern to increase revenue and reduce water use: Application of linear programming to Arjan Plain in Fars Province." *Agriculture*, Vol. 7(No. 9): pp. 73. doi:10.3390/agriculture7090073.

Dekker, A. G. 1993. *Detection of optical water quality parameters for eutrophic waters by high resolution remote sensing*. PhD thesis. Amsterdam: Free Universit, Vrije Universiteit Amsterdam. Accessed 20 April 2020 https://research.vu.nl/ws/portalfiles/portal/62846616/complete+-dissertation.pdf

Devred, E., Turpie, K.R., Moses, W., Klemas, V.V., Moisan, T., Babin, M., Toro-Farmer, G., Forget, M.H., and Jo, Y.H. 2013. "Future retrievals of water column bio-optical properties using the hyperspectral infrared imager (HYSPIRI)." *Remote Sensing*, Vol. 5(No. 12): pp. 6812–6837. doi:10.3390/rs5126812.

El-Alem, A., Chokmani, K., Laurion, I., and El-Adlouni, S.E. 2012. "Comparative analysis of four models to estimate chlorophyll-a concentration in case-2 waters using MODerate Resolution Imaging Spectroradiometer (MODIS) imagery." *Remote Sensing*, Vol. 4(No. 8): pp. 2373–2400. doi:10.3390/rs4082373.

Gitelson, A. 1992. "The peak near 700 nm on radiance spectra of algae and water: Relationships of its magnitude and position with chlorophyll concentration." *International Journal of Remote Sensing*, Vol. 13(No. 17): pp. 3367–3373. doi:10.1080/01431169208904125.

Gitelson, A.A., Gurlin, D., Moses, W.J., and Barrow, T. 2009. "A bio-optical algorithm for the remote estimation of the chlorophyll-a concentration in case 2 waters."

Environmental Research Letters, Vol. 4(No. 4): pp. 045003. doi:10.1088/1748-9326/4/4/045003.

Gordon, H.R., Brown, O.B., Evans, R.H., Brown, J.W., Smith, R.C., Baker, K.S., and Clark, D.K. 1988. "Semianalytic radiance model of ocean color." *Journal of Geophysical Research*, Vol. 93(No. D9): pp. 10909–10924. doi:10.1029/JD093iD09p10909.

Gordon, H.R., and Morel, A.Y. 2012. *Remote Assessment of Ocean Color for Interpretation of Satellite Visible Imagery: A Review*. Vol. 4. New York: Springer Science & Business Media. doi:10.1007/978-1-4684-6280-7.

Gordon, H.R., Brown, O.B., and Jacobs, M.M. 1975. "Computed relationships between the inherent and apparent optical properties of a flat homogeneous ocean." *Applied Optics*, Vol. 14(No. 2): pp. 417–427. doi:10.1364/AO.14.000417.

Gower, J., Doerffer, R., and Borstad, G. 1999. "Interpretation of the 685nm peak in water leaving radiance spectra in terms of putrescence, absorption and scattering, and its observation by MERIS." *International Journal of Remote Sensing*, Vol. 20(No. 9): pp. 1771–1786. doi:10.1080/014311699212470.

Gower, J., King, S., and Goncalves, P. 2008. "Global monitoring of plankton blooms using MERIS mci." *International Journal of Remote Sensing*, Vol. 29(No. 21): pp. 6209–6216. doi:10.1080/01431160802178110.

Gower, J., King, S., Borstad, G., and Brown, L. 2005. "Detection of intense plankton blooms using the 709 nm band of the MERIS imaging spectrometer." *International Journal of Remote Sensing*, Vol. 26(No. 9): pp. 2005–2012. doi:10.1080/01431160500075857.

Gower, J., King, S., Yan, W., Borstad, G., and Brown, L. 2003. "Use of the 709 nm band of meris to detect intense plankton blooms and other conditions in coastal waters." Proceedings of MERIS User Workshop, Frascati, Italy, 10–13 November 2003.

Hill, V.J., Zimmerman, R.C., Bissett, W.P., Dierssen, H., and Kohler, D.D. 2014. "Evaluating light availability, seagrass biomass, and productivity using hyperspectral airborne remote sensing in Saint Joseph's Bay." *Estuaries and Coasts*, Vol. 37(No. 6): pp. 1467–1489. 2014. doi:10.1007/s12237-013-9764-3.

Jerlov, N. G. 1976. *Marine Optics*. Vol. 14. Amsterdam: Elsevier.

Kahru, M., Mitchell, B.G., Diaz, A., and Miura, M. 2004. "MODIS detects a devastating algal bloom in Paracas Bay, Peru." *Eos Transactions American Geophysical Union*, Vol. 85(No. 45): pp. 465–472. doi:10.1029/2004EO450002.

Kutser, T. 2004. "Quantitative detection of chlorophyll in cyanobacterial blooms by satellite remote sensing." *Limnology and Oceanography*, Vol. 49(No. 6): pp. 2179–2189. doi:10.4319/lo.2004.49.6.2179.

Kutser, T., Herlevi, A., Kallio, K., and Arst, H. 2001. "A hyperspectral model for interpretation of passive optical remote sensing data from turbid lakes." *The Science of the Total Environment*, Vol. 268(No. 1–3): pp. 47–58. doi:10.1016/S0048-9697(00)00682-3.

Kutser, T., Pierson, D.C., Kallio, K.Y., Reinart, A., and Sobek, S. 2005. "Mapping Lake CDOM by satellite remote sensing." *Remote Sensing of Environment*, Vol. 94(No. 4): pp. 535–540. doi:10.1016/j.rse.2004.11.009.

Ledesma, M.M., Bonansea, M., Ledesma, C.R., Rodríguez, C., Carreño, J., and Pinotti, L. 2019. "Estimation of chlorophyll-a concentration using Landsat-8 in the Cassaffousth reservoir." *Water Supply*, Vol. 19(No. 7): pp. 2021–2027. doi:10.2166/ws.2019.080.

Letelier, R.M., and Abbott, M.R. 1996. "An analysis of chlorophyll fluorescence algorithms for the moderate resolution imaging spectrometer (modis)." *Remote Sensing of Environment*, Vol. 58(No. 2): pp. 215–223. doi:10.1016/S0034-4257(96)00073-9.

Maccoux, M.J., Dove, A., Backus, S.M., and Dolan, D.M. 2016. "Total and soluble reactive phosphorus loadings to Lake Erie: A detailed accounting by year, basin, country, and tributary." *Journal of Great Lakes Research*, Vol. 42(No. 6): pp. 1151–1165. doi:10.1016/j.jglr.2016.08.005.

Matthews, M.W. 2011. "A current review of empirical procedures of remote sensing in inland and near-coastal transitional waters." *International Journal of Remote Sensing*, Vol. 32(No. 21): pp. 6855–6899. doi:10.1080/01431161.2010.512947.

Matthews, M.W., Bernard, S., and Robertson, L. 2012. "An algorithm for detecting trophic status (chlorophyll-a), cyanobacterial-dominance, surface scums and floating vegetation in inland and coastal waters." *Remote Sensing of Environment*, Vol. 124: pp.637–652. doi:10.1016/j.rse.2012.05.032.

McKee, D., Cunningham, A., Wright, D., and Hay, L. 2007. "Potential impacts of nonalgal materials on water-leaving sun induced chlorophyll fluorescence signals in coastal waters." *Applied Optics*, Vol. 46(No. 31): pp. 7720–7729. doi:10.1364/AO.46.007720.

Mobley, C.D., and Sundman, L. 2001. *Hydrolight 4.2, Users Guide*, pp. 87. Redmond: Sequoia Scientific.

Mobley, C.D. 1995. "The optical properties of water." In *Handbook of Optics*, edited by M. Bass, Vol. 1, pp. 43–41.

Morel, A., and Prieur, L. 1977. "Analysis of variations in ocean color." *Limnology and Oceanography*, Vol. 22(No. 4): pp. 709–722. doi:10.4319/lo.1977.22.4.0709.

Moses, W.J., Gitelson, A.A., Berdnikov, S., and Povazhnyy, V. 2009. "Satellite estimation of chlorophyll-a concentration using the red and NIR bands of meristhe azov sea case study." *IEEE Geoscience and Remote Sensing Letters*, Vol. 6(No. 4): pp. 845–849. doi:10.1109/LGRS.2009.2026657.

Nguyen, M.V., Lin, C.H., Chu, H.J., Jaelani, L.M., and Syariz, M.A. 2019. "Spectral feature selection optimization for water quality estimation." *International Journal of Environmental Research and Public Health*, Vol. 17 (No. 1): pp. 272. doi:10.3390/ijerph17010272.

Odermatt, D., Gitelson, A., Brando, V.E., and Schaepman, M. 2012. "Review of constituent retrieval in optically deep and complex waters from satellite imagery." *Remote Sensing of Environment*, Vol. 118: pp. 116–126. doi:10.1016/j.rse.2011.11.013.

Olmanson, L.G., Bauer, M.E., and Brezonik, P.L. 2008. "A 20-year Landsat water clarity census of Minnesota's 10,000 lakes." *Remote Sensing of Environment*, Vol. 112(No. 11): pp. 4086–4097. doi:10.1016/j.rse.2007.12.013.

Olmanson, L.G., Brezonik, P.L., and Bauer, M.E. 2015. "Remote sensing for regional lake water quality assessment: Capabilities and limitations of current and upcoming satellite systems." In *Advances in Watershed Science*

and Assessment, edited by T. Younos and T.E. Parece, 111–140. Cham: Springer. doi:10.1007/978-3-319-14212-8_5.

Pal, S., Gregory-Eaves, I., and Pick, F. 2015. "Temporal trends in cyanobacteria revealed through DNA and pigment analyses of temperate lake sediment cores." *Journal of Paleolimnology*, Vol. 54(No. 1): pp. 87–101. 2015. doi:10.1007/s10933-015-9839-1.

Palmer, S.C., Kutser, T., and Hunter, P.D. 2015. "Remote sensing of inland waters: Challenges, progress and future directions." *Remote Sensing of Environment*, Vol. 157: pp. 1–8. doi:10.1016/j.rse.2014.09.021.

Stramski, D., Bricaud, A., and Morel, A. 2001. "Modeling the inherent optical properties of the ocean based on the detailed composition of the planktonic community." *Applied Optics*, Vol. 40(No. 18): pp. 2929–2945. doi:10.1364/AO.40.002929.

Tao, B., Mao, Z., Pan, D., Shen, Y., Zhu, Q., and Chen, J. 2013. "Inuence of bio-optical parameter variability on the reectance peak position in the red band of algal bloom waters." *Ecological Informatics*, Vol. 16: pp. 17–24. doi:10.1016/j.ecoinf.2013.04.005.

Tebbs, E., Remedios, J., and Harper, D. 2013. "Remote sensing of chlorophyll-a as a measure of cyanobacterial biomass in lake bogoria, a hypertrophic, saline-alkaline, Amingo lake, using Landsat ETM." *Remote Sensing of Environment*, Vol. 135: pp. 92–106. doi:10.1016/j.rse.2013.03.024.

Toming, K., Kutser, T., Laas, A., Sepp, M., Paavel, B., and Noges, T. 2016. "First experiences in mapping lake water quality parameters with Sentinel-2 MSI imagery." *Remote Sensing*, Vol. 8(No. 8): pp. 640. doi:10.3390/rs8080640.

Toming, K., Kutser, T., Uiboupin, R., Arikas, A., Vahter, K., and Paavel, B. 2017. "Mapping water quality parameters with sentinel-3 ocean and land colour instrument imagery in the Baltic Sea." *Remote Sensing*, Vol. 10(No. 9): pp. 1070. doi:10.3390/rs9101070.

Urquhart, E.A., Schaeffer, B.A., Stumpf, R.P., Loftin, K.A., and Werdell, P.J. 2017. "A method for examining temporal changes in cyanobacterial harmful algal bloom spatial extent using satellite remote sensing." *Algae Harmful*, Vol. 67: pp. 144–152. doi:10.1016/j.hal.2017.06.001.

Wang, M., and Shi, W. 2007. "The NIR-SWIR combined atmospheric correction approach for MODIS ocean color data processing." *Optics Express*, Vol. 15(No. 24): pp. 15722–15733. doi:10.1364/OE.15.015722.

Witter, D.L., Ortiz, J.D., Palm, S., Heath, R.T., and Budd, J.W. 2009. "Assessing the application of seawifs ocean color algorithms to lake Erie." *Journal of Great Lakes Research*, Vol. 35(No. 3): pp. 361–370. doi:10.1016/j.jglr.2009.03.002.